Mechanistic Studies of the Biosynthesis of Paratose: Purification and Characterization of CDP-paratose Synthase†

Tina M. Hallis, Yenyoung Lei, Nanette L. S. Que, and Hung-wen Liu*

Department of Chemistry, University of Minnesota, Minneapolis, Minnesota 55455

Received October 15, 1997; Revised Manuscript Received December 18, 1997

ABSTRACT: The 3,6-dideoxyhexoses can be found in the cell wall lipopolysaccharide of Gram-negative bacteria, where they have been shown to be the dominant antigenic determinants. All naturally occurring 3,6-dideoxyhexoses, with colitose as the only exception, are biosynthesized via a complex pathway that begins with CDP-D-glucose. Included in this pathway is CDP-paratose synthase, an essential enzyme in the formation of the 3,6-dideoxy sugars, CDP-paratose and CDP-tyvelose. Recently, the gene encoding CDP-paratose synthase in *Salmonella typhi*, *rfbS*, has been identified and sequenced [Verma, N., and Reeves, P. (1989) *J. Bacteriol. 171*, 5694−5701]. On the basis of this information, we have amplified the *rfbS* gene by polymerase chain reaction (PCR) from *S. typhi* and cloned this gene into a pET-24(+) vector. Expression and purification of CDP-paratose synthase have allowed us to fully characterize the catalytic properties of this enzyme, which is a homodimeric protein with a preference for NADPH over NADH. It catalyzes the stereospecific hydride transfer of the *pro-S* hydrogen from the C-4′ position of the reduced coenzyme to C-4 of the substrate, CDP-3,6-dideoxy-D-*glycero*-D-*glycero*-4-hexulose. The overall equilibrium of this catalysis greatly favors the formation of the reduced sugar product and the oxidized coenzyme. Interestingly, this enzyme also exhibits a high affinity for NADPH with a much smaller dissociation constant (K_{ia}) of 0.005 ± 0.002 μM compared to the K_m of 26 ± 8 μM for NADPH. While this unusual property complicated the interpretation of the kinetic data, the kinetic mechanism of CDP-paratose synthase as explored by the combination of bisubstrate kinetic analysis, product inhibition studies, and dead-end competitive inhibition studies is most consistent with a Theorell−Chance mechanism. The present study on CDP-paratose synthase, a likely new member of the short-chain dehydrogenase family, represents the first detailed characterization of this type of ketohexose reductase, many of which may share similar properties with CDP-paratose synthase.

Deoxy sugars with a variety of intriguing biological activities are found ubiquitously in nature (*1*−*3*). These unusual carbohydrates are derived from common sugars by the replacement of one or more hydroxyl groups with hydrogens, and such a substitution generally causes a fundamental change in their characteristics and metabolism. The conversion of ribonucleotide to 2-deoxyribonucleotide is a well-documented example; however, a more infrequent occurrence is that of the 3,6-dideoxyhexoses. These distinctive sugars are commonly an important constituent of the O-antigen of lipopolysaccharides (LPSs),[1] which are part of the outer membrane of Gram-negative bacteria (*4*−*6*). It has been shown that the immunological specificities of different Gram-negative strains are mainly determined by the sugars found at the nonreducing end of the O-antigen repeat units where 3,6-dideoxy sugars usually reside (*7*−*8*). Thus, 3,6-dideoxy sugars have been referred to as immunodominant sugars or antigenic determinants in bacteria. Out of the eight possible stereoisomers of 3,6-dideoxyhexoses, only five have been detected in nature, all in the family of *Enterobacteriaceae* (*7*, *9*).

Inspired by their limited occurrence in nature and their important immunological activities, substantial efforts have been devoted to exploring the biosynthesis of 3,6-dideoxyhexoses (*10*−*16*). Four out of the five naturally occurring 3,6-dideoxy sugars—abequose, ascarylose, paratose, and tyvelose—are derived from CDP-D-glucose (**2**) as shown in Scheme 1, while the fifth, colitose, arises from GDP-D-mannose (*17*). Although the precursors of these dideoxy sugars have been well defined and possible routes for their formation have been postulated, the only pathway that has been studied in detail at the enzymatic level is that of CDP-ascarylose (*16*). This complex biosynthetic pathway begins with the coupling of glucose 1-phosphate (**1**) with CTP catalyzed by D-glucose-1-phosphate cytidylyltransferase (E_p) to give CDP-D-glucose (**2**) (*18*). This is followed by an

† Supported by NIH Grants GM35906 and GM54346. T.M.H. is a trainee of a NIGMS Biotechnology Training Grant (2 T32 GM08347).

* To whom correspondence should be addressed.

[1] Abbreviations: ADP, adenosine 5′-diphosphate; CDP, cytidine 5′-diphosphate; CTP, cytidine 5′-triphosphate; DEAE, diethylaminoethyl; E_1, CDP-6-deoxy-D-*glycero*-L-*threo*-4-hexulose 3-dehydrase; E_3, CDP-6-deoxy-D-*glycero*-L-*threo*-4-hexulose 3-dehydrase reductase; E_{od}, CDP-D-glucose 4,6-dehydratase; E_p, α-D-glucose-1-phosphate cytidylyltransferase; FPLC, fast protein liquid chromatography; IPTG, isopropyl thiogalactoside; LPS, lipopolysaccharide; NAD^+, β-nicotinamide adenine dinucleotide; NADH, β-nicotinamide adenine dinucleotide, reduced form; $NADP^+$, β-nicotinamide adenine dinucleotide phosphate; NADPH, β-nicotinamide adenine dinucleotide phosphate, reduced form; PAGE, polyacrylamide gel electrophoresis; PCR, polymerase chain reaction; SDS, sodium dodecyl sulfate; UV, ultraviolet; GCG, Genetics Computer Group, Inc.

S0006-2960(97)02552-X CCC: $15.00
Published on Web 03/13/1998

Scheme 1

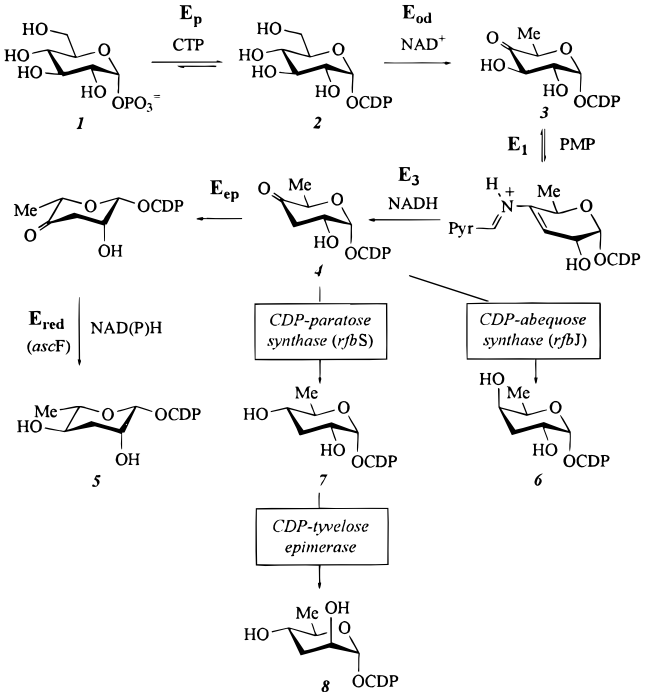

intramolecular oxidation−reduction catalyzed by NAD^+-dependent CDP-D-glucose 4,6-dehydratase (E_{od}) (*19*, *20*). The resulting product, CDP-6-deoxy-D-*glycero*-L-*threo*-4-hexulose (**3**), is then converted to CDP-3,6-dideoxy-D-*glycero*-D-*glycero*-4-hexulose (**4**) in two consecutive steps mediated by CDP-6-deoxy-D-*glycero*-L-*threo*-4-hexulose-3-dehydrase (E_1) (*12*, *21*−*24*) and E_1 reductase (E_3) (*13*, *25*−*28*). Compound **4** is the common precursor of all four dideoxy sugars that originate from glucose 1-phosphate (*16*). Subsequent production of CDP-ascarylose (**5**) requires an epimerase and a reductase (*29*), while CDP-abequose (**6**) and CDP-paratose (**7**) are each formed from **4** by a stereospecific reduction. The intermediacy of CDP-paratose (**7**) in the biosynthesis of CDP-tyvelose (**8**) has been established in both *Yersinia* (formerly know as *Pasturella*) and *Salmonella* (*30*−*32*). Thus, tyvelose is unique in that it is derived from another 3,6-dideoxyhexose, and the conversion is accomplished by an epimerase (*16*).

In this paper, we present the overexpression, purification, and characterization of CDP-paratose synthase, which converts **4** to CDP-paratose (**7**). As mentioned above, this enzyme is essential not only for the production of CDP-paratose but also for the biosynthesis of CDP-tyvelose (**8**). Currently, the biochemical information on this type of hexulose reductase is scarce. Our investigations included various inhibition studies, which indicated that CDP-paratose synthase follows a Theorell−Chance mechanism, an ordered mechanism with product release as its rate-limiting step. This is analogous to the catalysis of many dehydrogenases that also follow ordered mechanisms and often have coenzyme release as their rate-limiting step (*33*). Interestingly, our results show that the enzyme has a strong affinity for NADPH with a K_{ia} much lower than the K_m for this same cosubstrate, and the overall equilibrium greatly favors the formation of the reduced sugar product. Since CDP-paratose synthase is likely to be prototypical for hexulose reductases, these properties may also be characteristic for this class of enzymes.

EXPERIMENTAL PROCEDURES

General. Protein concentrations were determined by the procedure of Bradford (*34*) using bovine serum albumin as the standard. The NMR spectra were acquired on a Varian Unity 300 spectrometer, and all UV spectra were taken on a Beckman DU650 spectrophotometer. Fluorometric experiments were performed on a Perkin-Elmer LS50B spectrofluorometer. N-Terminal sequencing of purified CDP-paratose synthase was carried out by the University of Minnesota Microchemical Facility in the Institute of Human Genetics.

Salmonella typhi Genomic DNA Isolation. The bacterial strain *S. typhi* (ATCC no. 19430) was purchased from ATCC (Bethesda, MD). Cells from an overnight liquid culture (3% tryptic soy broth, w/v) were harvested by centrifugation at 4000*g* for 10 min at 4 °C. The cells were resuspended in TE buffer (10 mM Tris-HCl and 1 mM EDTA, pH 7.5) and incubated with 1% SDS and 1 mg of proteinase K for 1 h at 37 °C. To this solution were added NaCl and a 10% w/v solution of CTAB/NaCl (cetylhexadecyltrimethylammonium bromide in 0.7 M NaCl) to give a final concentration of 760 mM and 1%, respectively. The resulting mixture was incubated at 65 °C for 20 min and was then extracted with an equal volume of chloroform/isoamyl alcohol (24:1). After centrifugation at 6000*g* for 10 min, the viscous aqueous phase was collected and incubated with DNase-free RNase (2 units/mL of original culture) for 30 min at 37 °C. Another chloroform/isoamyl alcohol extraction was performed, followed by extraction with phenol/chloroform/isoamyl alcohol (25:24:1). The aqueous phase was collected, and 2-propanol was then used to precipitate the DNA. The DNA pellet, collected by centrifugation, was washed with cold 70% ethanol and resuspended in TE buffer. The concentration of DNA was determined by measuring the A_{260} (1 OD at 260 nm = 50 μg/mL for double-stranded DNA), and the purity was assessed on the basis of the A_{260}/A_{280} ratio.

Gene Amplification and Cloning. The sequence of the *rfbS* gene in *S. typhi* has been reported (*32*), and this information allowed the design of oligonucleotide primers complementary to the sequence at each end of the gene. The start primer, 5′-CGCGC**GAATTC**AGGAGGAAATTTAAAATGAAAA-TTCTAATAATGG-3′, contained a *Eco*RI restriction site (in bold), an *Escherichia coli* ribosome binding sequence, a TA-rich region, and the codons for the first six amino acid residues of the desired enzyme. The halt primer, 5′-GCGC**AAGCTT**TCATTTCCCTTCCTC-3′, introduced a *Hin*dIII restriction site (in bold) immediately downstream from the *rfbS* gene stop codon. These primers were used to amplify the *rfbS* gene from the genomic *S. typhi* DNA by PCR (*35*). The PCR-amplified DNA fragment was purified, digested with *Eco*RI and *Hin*dIII, and ligated into the *Eco*RI/*Hin*dIII sites of the transcription vector, pET-24+ (Novagen) to give pTHS-3. This recombinant plasmid was isolated and was used to transform *E. coli* HB101. Positive clones were identified by digestion of the plasmid DNA with *Eco*RI and *Hin*dIII and visualization of the excised insert by staining an agarose gel of the DNA with ethidium bromide after electrophoresis. The plasmid DNA from positive clones was used to transform *E. coli* BL21(DE3). The general methods and protocols for recombinant DNA manipulations were as described by Sambrook et al. (*36*).

DNA Sequencing. Nucleotide sequencing of the *rfb*S gene by the dideoxy chain termination method (*37*) was carried out directly on double-stranded DNA using commercially available M13 forward and reverse primers and several synthetic primers matching the gene's internal sequence.

Polyacrylamide Gel Electrophoresis. The level of expression and the solubility of the gene product and its relative abundance in the crude protein extract were assessed by SDS−polyacrylamide gel electrophoresis. Electrophoresis was carried out in the discontinuous buffer system of Laemmli (*38*), and the separating gel and stacking gel were 12% and 4% polyacrylamide, respectively. Prior to electrophoresis, protein samples were heated in 62.5 mM Tris-HCl buffer (pH 6.8) containing 10% glycerol, 2% SDS, 5% β-mercaptoethanol, and 0.0025% bromophenol blue. Electrophoresis of the heated samples was run in 25 mM Tris-HCl, 192 mM glycine, and 0.1% SDS (pH 8.3) at 25 mA. Gels were stained with Coomassie blue (*39*) and destained with acetic acid/ethanol/water (15:20:165 by volume).

Growth of E. coli (pTHS-3) Cells. An overnight culture of *E. coli* BL21(DE3)/pTHS-3, grown in Luria−Bertani (LB) medium supplemented with kanamycin (35 μg/mL) at 37 °C, was diluted with 2 L (0.1% v/v) of the same medium and incubated at 37 °C until the OD_{600} reached 0.5. The culture was cooled to room temperature and induced with 0.08 mM IPTG, after which the incubation was continued for an additional 15 h at 25 °C. The cells were harvested by centrifugation (6600*g*, 30 min), washed with 250 mL of 50 mM potassium phosphate buffer containing 0.4 M NaCl, pH 7.5, collected again by centrifugation (6600*g*, 30 min), and stored at −20 °C. The typical yield was 5 g of wet cells per liter of culture.

Enzyme Purification. The purification was carried out at 4 °C, except for the FPLC step, which was run at room temperature.

Step 1: Crude Extract. Thawed cells were resuspended in 100 mL of 20 mM Tris-HCl buffer, pH 7.5, and disrupted by sonication in five 40-s bursts with a 1-min cooling period between each blast. Cell debris was removed by centrifugation (14000*g*, 30 min), and the supernatant was treated with solid ammonium sulfate added portionwise over 1 h to 75% saturation. This cloudy solution was stirred for an additional hour, and the precipitated proteins were collected by centrifugation (12000*g*, 20 min). The sedimented proteins were resuspended in 40 mL of 20 mM Tris-HCl buffer, pH 7.5, and dialyzed against 2 L of the same buffer for 4 h with 3 changes of buffer.

Step 2: DEAE-Sepharose CL6B Chromatography. The dialysate from step 1 was loaded onto a column of DEAE-Sepharose CL6B (2.5 × 20 cm) preequilibrated with 20 mM Tris-HCl buffer, pH 7.5. After loading, the column was washed with 50 mL of the same buffer, followed by elution with a linear gradient of NaCl from 0 to 0.3 M in 20 mM Tris-HCl buffer, pH 7.5 (1 L total volume). The flow rate was 1.4 mL/min, and 13-mL fractions were collected during the gradient elution. The active fractions were pooled, concentrated by ultrafiltration on an Amicon concentrator using a YM 10 membrane (Amicon), and desalted using 20 mM Tris-HCl buffer, pH 7.5.

Step 3: FPLC MonoQ Chromatography. The enzyme solution from step 2 was further purified by FPLC with a MonoQ HR (10/10) column using solvent systems A (20 mM Tris-HCl buffer, pH 7.5) and B (A plus 500 mM NaCl). The elution profile was initiated with 0% B from 0 to 5 min, followed by a linear gradient of 30% to 60% B from 5 to 28 min, and concluded with a 5-min wash at 100% B. The flow rate was 3 mL/min. The active fractions were pooled, concentrated by ultrafiltration as before, desalted using 20 mM Tris-HCl buffer (pH 7.5), and stored at −80 °C.

Molecular Mass Determination. The native molecular mass of CDP-paratose synthase was determined by gel filtration performed on a Pharmacia FPLC Superdex 200 HR 10/30 column with 10 mM Tris-HCl buffer (pH 7.5) at a flow rate of 1 mL/min. The column was calibrated with protein standards (Sigma): β-amylase (200 kDa), bovine serum albumin (66 kDa), carbonic anhydrase (29 kDa), and cytochrome *c* (12 kDa). The data were analyzed by the method of Andrews (*40*). The subunit molecular mass was estimated by SDS−PAGE as described by Laemmli (*38*). Protein standards included α-lactalbumin (14 kDa), trypsin inhibitor (20 kDa), trypsinogen (24 kDa), carbonic anhydrase (29 kDa), glyceraldehyde-3-phosphate dehydrogenase (36 kDa), egg albumin (45 kDa), and bovine serum albumin (66 kDa).

Enzyme Assay. CDP-paratose synthase activity was determined spectrophotometrically by following the consumption of NADPH at 340 nm ($\epsilon_{340} = 6220\ M^{-1}\ cm^{-1}$). The standard assay solution contained 525 μL of 200 mM potassium phosphate buffer, pH 7.0, 35 μM NADPH, 150 μM CDP-3,6-dideoxy-D-*glycero*-D-*glycero*-4-hexulose (**4**), and an appropriate amount of enzyme (∼0.1 μg). The cuvette containing the assay mixture was thermostated at 25 °C, and the reaction was initiated by the addition of 5 μL of enzyme solution. One unit of enzyme activity is defined as the consumption of 1 μmol of NADPH per minute under the assay conditions, and specific activities are reported as units per milligram of protein. For the kinetic analysis, pure enzyme was diluted to 9 μg/mL with 200 mM potassium phosphate buffer, pH 7.0, supplemented with 0.5% BSA. Inhibition kinetics were performed by using the same assay conditions with addition of the appropriate inhibitor. It should be pointed out that over time the CDP-3,6-dideoxy-D-*glycero*-D-*glycero*-4-hexulose slowly decomposes by cleavage of the diphosphate bond. Therefore, the actual concentration of the sugar substrate used in the kinetic experiments was determined by HPLC using the procedure described below for the synthesis of CDP-3,6-dideoxy-D-*glycero*-D-*glycero*-4-[4-^{13}C]hexulose (**4**).

Synthesis of CDP-3,6-dideoxy-D-glycero-D-glycero-4-hexulose (4). The substrate for CDP-paratose synthase was prepared from glucose 1-phosphate (**1**) using enzymes previously overexpressed and purified in our laboratory (*18*, *24*, *27*). The 2-mL incubation mixture contained 150 μmol of glucose 1-phosphate, 80 μmol of CTP, 20 μmol of $MgCl_2$, 140 units of α-D-glucose-1-phosphate cytidylyltransferase (E_p), 370 units of CDP-D-glucose 4,6-dehydratase (E_{od}), and 20 mM Tris-HCl buffer (pH 7.5). The reaction was incubated for 2.5 h at room temperature, and the yield of the product, CDP-6-deoxy-D-*glycero*-L-*threo*-4-hexulose (**3**), was determined spectrophotometrically at 320 nm under alkaline conditions (*12*). The E_p and E_{od} proteins were removed with a Centricon 10 microconcentrator (Amicon), and the filtrate was incubated with 70 μmol of NADH, 1.8 units of CDP-6-deoxy-D-*glycero*-L-*threo*-4-hexulose 3-dehydrase (E_1), and 50 units of E_1 reductase (E_3) for 2 h at room temperature.

The E_1 and E_3 proteins were removed with a Centricon 10 microconcentrator, and the hexulose product (**4**) was purified by a FPLC MonoQ HR (10/10) column using a gradient with water as solvent A and 500 mM NH_4HCO_3 as solvent B. The elution profile began with 0% B for 5 min, a linear gradient from 0 to 35% B from 5 to 35 min, and a final wash with 100% B for 5 min. The purified CDP-3,6-dideoxy-D-*glycero*-D-*glycero*-4-hexulose (**4**) was lyophilized and stored at −20 °C. The yield was 35 μmol (44%). Since the keto form of this compound is in equilibrium with its hydrate form at a ratio of 1:2, two sets of signals for the hexulose part are discernible in the ^{1}H NMR spectrum. ^{1}H NMR (D_2O, 300 MHz) δ 7.77 (1H, d, J = 7.6 Hz; cytidine H-6), 5.93 (1H, d, J = 7.6 Hz, cytidine H-5), 5.77 (1H, d, J = 3.9 Hz, cytidine H-1′), 4.0−4.3 (5H, m, cytidine H-2′, 3′, 4′, 5′), 5.50 (1H, dd, J = 6.6, 3.3 Hz, H-1 of keto form), 5.31 (1H, dd, J = 6.6, 3.3 Hz, H-1 of hydrate form), 4.35 (1H, q, J = 6.5 Hz, H-5 of keto form), 4.02 (1H, m, H-2 of keto form), 3.80 (1H, q, J = 6.3 Hz, H-5 of hydrate form), 3.69 (1H, m, H-2 of hydrate form), 2.60 (2H, broad d, J = 7.8 Hz, H-3 of keto form), 1.93 (1H, dd, J = 12.4, 4.8 Hz, H-3$_{eq}$ of hydrate form), 1.78 (1H, t, J = 12.4 Hz, H-3$_{ax}$ of hydrate form), 1.04 (3H, d, J = 6.5 Hz, 5-Me of keto form), 0.95 (3H, d, J = 6.3 Hz, 5-Me of hydrate form).

*Synthesis of CDP-3,6-dideoxy-D-glycero-D-glycero-4-[4-^{13}C]hexulose (**4**).* The 4-^{13}C-labeled substrate for CDP-paratose synthase was enzymatically synthesized from D-[4-^{13}C]glucose. The incubation mixture contained 28 μmol of D-[4-^{13}C]glucose (Cambridge Isotope Laboratories), 90 μmol of $MgSO_4$, 60 μmol of ATP, and 64 units of yeast hexokinase in 4 mL of 100 mM potassium phosphate buffer (pH 7.0). After an incubation of 1 h at room temperature, 20 μmol of $MgCl_2$, 150 units of inorganic pyrophosphatase, 31 μmol of CTP, 0.9 μmol of glucose 1,6-bisphosphate, 100 units of chicken phosphoglucomutase, and 85 units of E_p were added, and incubation was continued for 3 h at 30 °C. To this mixture was then added 370 units of E_{od}, and incubation was allowed to proceed for another 2 h at room temperature. After the proteins were removed with a Centricon 10 microconcentrator (Amicon), the filtrate was mixed with 18 μmol of NADH, 0.9 units of E_1, and 28 units of E_3 and incubated for 2 h at room temperature. At the end of the incubation, all proteins were removed with a Centricon 10 microconcentrator, and the sugar product was purified by HPLC with a Spherisorb S5 SAX semiprep column (1.0 × 25 cm) using a solvent system with water as solvent A and 400 mM potassium phosphate (pH 4.0) as solvent B. The elution followed a profile of 0−10% B from 0 to 5 min and a linear gradient of 10 to 50% B from 5 to 35 min. The column was then washed with 100% B for 5 min. The flow rate was 2.5 mL/min, and the absorbance was recorded at 270 nm. The purified sample was lyophilized and stored at −20 °C. The overall yield was 22%.

*Production and Characterization of CDP-paratose (**7**).* CDP-3,6-dideoxy-D-*glycero*-D-*glycero*-4-hexulose (**4**, 15 μmol) prepared earlier was incubated with 15 μmol of NADH and 1 unit of CDP-paratose synthase for 30 min at room temperature to produce CDP-paratose (**7**). The conversion was nearly quantitative on the basis of ^{1}H-NMR analysis. The product was purified using the same FPLC conditions as described above for the substrate purification. The identity of CDP-paratose was confirmed by ^{1}H and COSY NMR. ^{1}H NMR (D_2O, 300 MHz) δ 7.85 (1H, d, J = 7.6 Hz, cytidine H-6), 5.99 (1H, d, J = 7.6 Hz, cytidine H-5), 5.82 (1H, d, J = 4.0 Hz, cytidine H-1′), 5.30 (1H, dd, J = 3.2, 6.7 Hz, H-1), 4.22−4.02 (5H, m, cytidine H-2′, 3′, 4′, 5′), 3.68−3.59 (2H, m, H-2, 5), 3.20 (1H, ddd, J = 4.6, 11.5, 11.5 Hz, H-4), 1.97 (1H, ddd, J = 4.4, 4.4, 10.1 Hz, H-3$_{eq}$), 1.58 (1H, ddd, J = 11.7, 11.7, 10.2 Hz, H-3$_{ax}$), 1.06 (3H, d, J = 6.2 Hz, 5-Me).

Preparation of Stereospecifically Deuterated NADH. The (4*R*)-[4-^{2}H]NADH sample was prepared with NAD^+, [$^2H_6$]-ethanol, and yeast alcohol dehydrogenase (*41*, *42*). The labeled coenzyme was purified on a DEAE-Sepharose CL6B column using a linear gradient of 0 to 0.2 M $(NH_4)_2CO_3$, and fractions with A_{260}/A_{340} < 2.4 were pooled and lyophilized. The (4*S*)-[4-^{2}H]NADH sample was prepared with NAD^+, DTT, lipoamide, and lipoamide dehydrogenase in ^2H_2O, pD 8.5 (*43*), and purified as before by DEAE-Sepharose chromatography. NMR analysis of both products validated the chirality and also confirmed greater than 95% deuteration by comparing the peak integrals of H-2 and H-4 at δ 6.98 and 2.80, respectively.

Determination of Stereospecificity of Hydride Transfer from NADH.[2] The prepared (4*R*)- and (4*S*)-[4-^{2}H]NADH were each incubated with CDP-paratose synthase and CDP-3,6-dideoxy-D-*glycero*-D-*glycero*-4-hexulose (**4**). The 1-mL incubation mixture contained 7 μmol of labeled NADH, 10 μmol of sugar substrate (**4**), 1.8 mg (167 units) of CDP-paratose synthase, and 50 mM potassium phosphate buffer, pH 7.5. After incubation for 2 h at room temperature, the enzyme was removed with a Centricon 10 microconcentrator, and the resulting NAD^+ was purified using the same FPLC conditions as described above for the substrate purification. The purified NAD^+ was lyophilized, redissolved in ^2H_2O, and analyzed by ^{1}H NMR.

Equilibrium Constant. The K_{eq} equilibrium constant was calculated from eq 1. Three separate incubations containing different quantities of both products (108 μM CDP-paratose with 860 μM $NADP^+$, 213 μM CDP-paratose with 844 μM $NADP^+$, and 205 μM CDP-paratose with 1630 μM $NADP^+$) in potassium phosphate buffer (pH 8.0) were initiated with 45 μg of CDP-paratose synthase. Reactions were carried out at 25 °C and were monitored by the production of NADPH at 340 nm. The reaction was considered at equilibrium when the absorbance at 340 nm reached a plateau. The net change in absorption at 340 nm was used to calculate the concentration of each substrate and product, assuming a 1:1 stoichiometry for the production of NADPH and the consumption of CDP-paratose. The reported K_{eq} value was obtained by averaging these three measurements.

$$K_{eq} = \frac{[NADP^+][\text{CDP-paratose}]}{[NADPH][\mathbf{4}][H^+]} \quad (1)$$

Determination of Kinetic Parameters. Assays were carried out as described above. The kinetic measurements were analyzed by fitting the data to either of two equations for

[2] The determination of the stereospecificity of hydride transfer from NADH was performed before it was known that CDP-paratose synthase prefers NADPH by approximately 10-fold. The experiment was not repeated with NADPH since the enzyme can use NADH in the catalysis, and the stereospecificity for the hydride transfer from NADPH is not expected to differ from that of NADH.

bimolecular reaction mechanisms using a nonlinear least-squares program. Equation 2 is for a sequential mechanism in which K_{ia} is the dissociation constant for substrate A, K_{mA} is the Michaelis−Menten constant for substrate A, K_{mB} is the Michaelis−Menten constant for substrate B, and V is the maximum rate. The equation for a ping-pong mechanism is similar to eq 2, but without the $K_{ia}K_{mB}$ term in its denominator.

$$v = \frac{V[AB]}{K_{ia}K_{mB} + K_{mB}[A + K_{mA}[B] + [AB]]} \quad (2)$$

Slopes of Hanes−Woolf plots ([S]/v vs [S]) were calculated by linear regression, and kinetic parameters (K_{ia}, K_{mB}, K_{mA}, and V) were derived from replots of the slope against the reciprocal of the substrate concentration. Initial velocities were measured in duplicate at several nonsaturating concentrations of each substrate with each individual measurement plotted. The general approach to determining the kinetic mechanism is as described by Segel (*44*).

Competitive inhibition data were analyzed using eq 3 where K_m is the Michaelis−Menten constant for the substrate of interest and K_{is} is the slope inhibition constant. The y-intercepts from Hanes−Woolf plots of the inhibition data were replotted against the inhibitor concentration, and linear regression was used to obtain the inhibition constant K_{is}.

$$v = \frac{V[S]}{K_m(1 + (I/K_{is})) + [S]} \quad (3)$$

Determination of NADPH Binding Affinity with CDP-paratose Synthase. The affinity (K_d) of CDP-paratose synthase for NADPH was determined by monitoring the increase in the NADPH fluorescence upon binding with CDP-paratose synthase. The excitation wavelength was set at 360 nm, and the emission of fluorescence at 450 nm was monitored, with both the excitation and emission slits set at 5 nm. In each experiment, 2.2 μM CDP-paratose synthase (functional dimer) was used, while the NADPH concentration was varied from 0 to 25 μM. All measurements were carried out at 25 °C. A control without enzyme for the respective NADPH solution used in each titration was also run to estimate the fluorescence of the unbound NADPH so that each of the measured values at 450 nm was corrected by subtracting the contribution from unbound NADPH. From the measured fluorescence intensity I at a given NADPH concentration, the average number v of moles of NADPH bound per mole of protein was deduced by using $v = n(I - I_i)/(I_m - I_i)$, where n represents the number of coenzyme binding sites; I_i, the initial fluorescence of the NADPH control without enzyme; and I_m, the maximum fluorescence when the NADPH concentration is saturating. The free NADPH concentration x (or $[NADPH]_f$) was estimated using $x = [NADPH]_t - n[E]_t$, in which $[NADPH]_t$ and $[E]_t$ represent the total NADPH and enzyme concentrations, respectively. A nonlinear least-squares procedure was used

$$v = \frac{\frac{x}{K_1} + \frac{2x^2}{K_1K_2} + ... + \frac{nx^n}{K_1K_2...K_n}}{1 + \frac{x}{K_1} + \frac{x^2}{K_1K_2} + ... + \frac{x^n}{K_1K_2...K_n}} \quad (4)$$

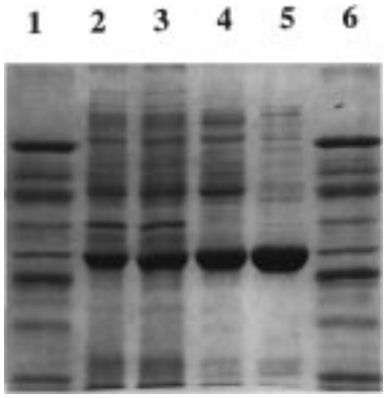

FIGURE 1: SDS−PAGE gel showing the purification of CDP-paratose synthase from *E. coli* BL21(DE3)/pTHS-3 at each step. Lanes: 1, molecular weight markers (from top, bovine serum albumin, 66 kDa; egg albumin, 45 kDa; glyceraldehyde-3-phosphate dehydrogenase, 36 kDa; carbonic anhydrase, 29 kDa; trypsinogen, 24 kDa; trypsin inhibitor, 20.1 kDa; α-lactalbumin, 14.2 kDa); 2, cell-free extract; 3, ammonium sulfate precipitate resuspended and dialyzed; 4, pooled DEAE-Sepharose fractions; 5, pooled MonoQ fractions.

to fit v and x to the Adair−Klotz equation (eq 4) (*45*, *46*) to determine the dissociation constants, K_1, K_2, and so on.

RESULTS

Cloning and Overexpression of the rfbS Gene. Due to the scarcity of CDP-paratose synthase in the wild-type bacterial sources, we decided to pursue the construction of an overexpression system for the synthase. The recently reported sequence of the *rfbS* gene from *S. typhi* (*32*) facilitated the first step of this task. Primers corresponding to the sequence at the 5′ and 3′ ends of the *rfbS* gene were used to amplify this gene by PCR from the genomic DNA of *S. typhi.* Since a ribosomal binding site was part of the PCR start primer, the amplified insert was cloned directly into a transcription vector, pET-24(+), which carries a T7/*lac* promoter. The sequence of the insert in the recombinant construct, pTHS-3, was verified by the Sanger method (*37*) to ensure that no misincorporation errors occurred during amplification.

Purification and Characterization of CDP-paratose Synthase. Induction of BL21(DE3) cells containing the pTHS-3 construct with IPTG led to the overexpression of the desired *rfbS* gene product. Unfortunately, the expressed protein was obtained as mostly inclusion bodies. This expression system, however, was fine-tuned for improved production of soluble protein by cooling the cell culture to room temperature prior to induction with a low level of IPTG (0.08 mM). As illustrated by the SDS−PAGE (Figure 1) and purification summary (Table 1), 170 mg of nearly homogeneous protein was obtained from 13 g of wet cells (2 L of culture) after only two chromatographic steps. N-Terminal sequence analysis confirmed that the first 10 amino acid residues (M-K-I-L-I-M-G-A-F-G) of this protein are identical with the translated *rfbS* sequence. Its subunit molecular mass of 29 kDa, revealed by SDS−PAGE, correlates well to the predicted value of 31 501 Da calculated from the deduced amino acid sequence. A molecular mass M_r of 55 kDa, estimated by gel filtration, indicates that the native CDP-paratose synthase exists as a homodimer. The electronic absorption spectrum of the purified enzyme shows a maxi-

Table 1: Purification of CDP-paratose Synthase from *E. coli* BL21(DE3)/pTHS-3

purification step	total protein[a] (mg)	total activity[b] (units)	sp activity (units/mg)	yield (%)	purification (fold)
crude[c]	1350	37 800	28	100	1
$(NH_4)_2SO_4$ ppt	1350	32 400	24	86	0.9
DEAE-Sepharose	605	28 800	48	76	1.7
MonoQ	170	15 800	93	42	3.3

[a] Determined using the Bradford dye-binding assay (Bio-Rad). [b] One unit = 1 μmol NADPH consumption/min. [c] Obtained from 13 g of wet cells.

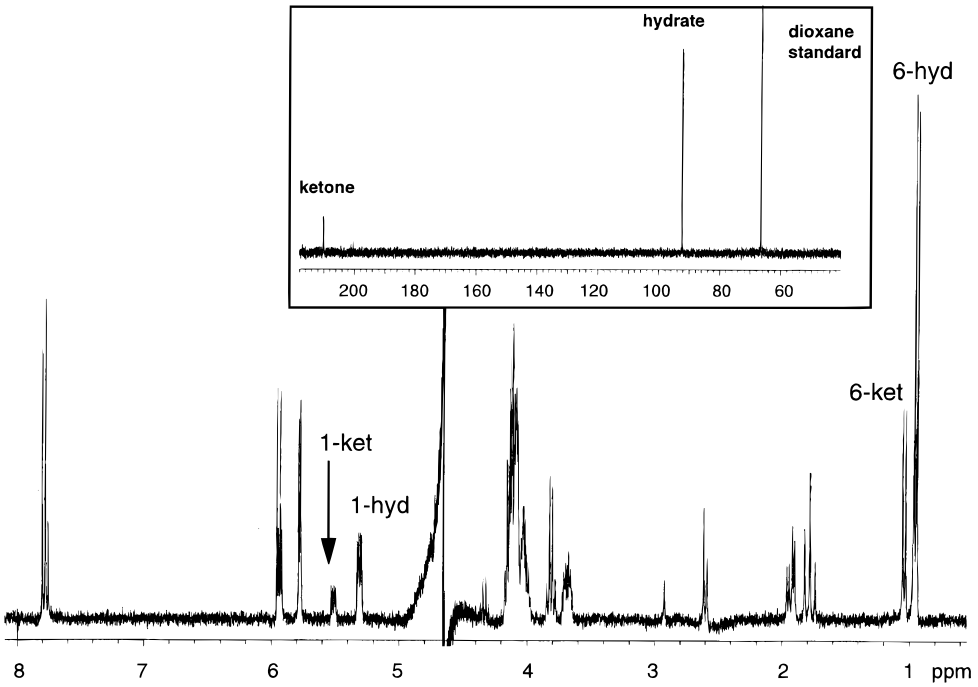

FIGURE 2: ^{1}H NMR spectrum of CDP-3,6-dideoxy-D-*glycero*-D-*glycero*-4-hexulose (**4**). The signals corresponding to the hydrate and keto forms of the H-1 and H-6 protons are labeled. The inset displays the ^{13}C NMR spectrum of CDP-3,6-dideoxy-D-*glycero*-D-*glycero*-4-hexulose enriched with ^{13}C at the C-4 position of the hexose.

mum at 280 nm. Since there is no absorbance above 300 nm, this enzyme does not contain bound cofactor(s) such as cytochrome, flavin, or pyrroloquinoline quinone, which have been found in some bacterial alcohol dehydrogenases (*47*). The concentrated CDP-paratose synthase can endure several freeze/thaw cycles before beginning to precipitate out of solution. When stored at −80 °C, the enzyme maintains its activity for at least 1 year. However, the synthase is very unstable at low protein concentration. Hence, when diluted samples were used for kinetic studies, the enzyme was stabilized by the addition of 0.5% BSA.

Synthesis and Characterization of the CDP-paratose Synthase Substrate. The enzymatic synthesis of the substrate, CDP-3,6-dideoxy-D-*glycero*-D-*glycero*-4-hexulose (**4**), from glucose 1-phosphate (**1**) followed an established sequence (*48*), and the required enzymes were purified from the overproducing strains previously constructed in our lab. Interestingly, the ^{1}H NMR spectrum of the highly purified **4** exhibits two sets of signals for the hexulose moiety, which are particularly apparent for the two C-5 methyl doublets at δ 0.95 and 1.04 and the two anomeric proton resonances at δ 5.31 and 5.50 (Figure 2). Such a doubling NMR pattern is indicative of the presence of two distinct forms of this compound in solution, and a comparison of the integration of the two C-5 methyl doublets revealed a ratio of 2:1 for these two species. Since the keto group of a hexulose can be hydrated, it is likely that these two species in equilibrium

Scheme 2

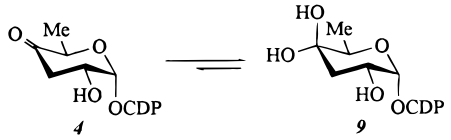

4 *9*

are **4** and its corresponding hydrate form (**9**) (Scheme 2). To verify this possibility, compound **4** enriched with ^{13}C at C-4 was prepared from D-[4-^{13}C]glucose. As expected, the labeled **4** exists in solution as two distinct forms on the basis of the two ^{13}C NMR signals at 210 and 92 ppm (Figure 2, inset). The chemical shifts of these two peaks are characteristic for a keto (in hexulose form) and a ketal carbon (in hydrate form), respectively. Judging from the intensity of the signals, it is clear that the hydrate form (**9**) is the dominant species of this mixture. The assignment of the corresponding proton signals of these two species in the ^{1}H NMR spectrum was facilited by COSY analysis. It was noted that there is a fairly rapid exchange of the C-3 protons resulting in deuterium incorporation at the equatorial position when **4** is dissolved in D_2O. These findings are in agreement with the results reported by Gould and Guo (*49*) for a cytosine glycoside having a similar 4-hexulose skeleton. The preference for exchange of the equatorial hydrogen at C-3 can be rationalized by considering the structure of the resulting enolate, whose bottom side is hindered by the axial CDP group.

Isolation and Characterization of the CDP-paratose Synthase Product. The reaction product of CDP-paratose synthase was purified by FPLC and confirmed to be CDP-paratose (**7**) by ^{1}H NMR. Since the product is not a hexulose, the existence of a keto−hydrate mixture is no longer an issue. This enzymatic conversion is nearly quantitative.

Stereospecificity of Hydride Transfer from NADH. The stereochemical course of the hydride transfer step was probed using stereospecifically labeled NADH. The enantiomeric purity of each labeled sample was estimated to be greater than 95% by ^{1}H NMR. The oxidized NAD^+ generated during the reaction was isolated and also analyzed by ^{1}H NMR. It was found that the signal for H-4 at δ 8.65 was retained in the NAD^+ species derived from incubation of (4*S*)-[4-^{2}H]NADH, indicating the transfer of the *pro-S* deuterium. On the contrary, incubation with (4*R*)-[4-^{2}H]-NADH resulted in retention of the deuterium on the nicotinamide ring, since the δ 8.65 signal was absent. Thus, the stereochemical preference of this enzyme with regard to the transfer of one of the diastereotopic methylene hydrogens at C-4 of the dihydronicotinamide ring was established to be *pro-S* stereospecific.

Equilibrium Constant. The reaction catalyzed by CDP-paratose synthase is a reversible process, but the calculated K_{eq} of 1.6×10^{12} M^{-1} at pH 8.0 indicates that the overall equilibrium strongly favors the reduction of CDP-3,6-dideoxy-D-*glycero*-D-*glycero*-4-hexulose (**4**). Due to such a strong preference for the reduced product, establishment of the equilibrium was initiated by using a mixture which contained only CDP-paratose and $NADP^+$. This approach enabled a more accurate determination of the NADPH concentration since the contribution of absorbance at 340 nm by the strong absorbance of large concentrations of $NADP^+$ at 280 nm was easier to subtract. Also, a pH of 8.0 was used for these reactions since this increased the final concentration of substrates (**4** and NADPH) and gave more reliable values for these concentrations. Therefore, the actual equilibrium constant for a pH of 7 would be even larger.

Kinetic Properties. During the development of the activity assay, optimum CDP-paratose synthase activity was observed when the buffer used was potassium phosphate at pH 7.0 and at 200 mM ionic strength. In addition, the synthase exhibits a much sharper reduction in activity in slightly acidic rather than alkaline conditions. The preference for NADPH over NADH by a factor of approximately 10 was also established on the basis of initial velocity rates.

Under the above optimal conditions, the K_m values were determined to be 26 ± 8 μM for NADPH and 255 ± 20 μM for CDP-3,6-dideoxy-D-*glycero*-D-*glycero*-4-hexulose (**4**), and the V_{max} was 190 ± 20 μmol min^{-1} mg^{-1}. Hanes−Woolf plots of initial velocities either as a function of NADPH concentration (10−150 μM) at several levels of CDP-3,6-dideoxy-D-*glycero*-D-*glycero*-4-hexulose concentration (50−290 μM) or as a function of CDP-3,6-dideoxy-D-*glycero*-D-*glycero*-4-hexulose concentration at several levels of NADPH concentration yielded lines which converged on or near the *y*-axis (Figure 3).

Product and Dead-End Inhibition Studies. To elucidate the kinetic mechanism of this enzyme, the effects of product inhibition on the catalysis were investigated. Our results indicate that $NADP^+$ (280 μM) is a mixed type or uncompetitive inhibitor with respect to CDP-3,6-dideoxy-D-*glycero*-D-*glycero*-4-hexulose (50−300 μM) and is a competitive inhibitor for NADPH (20 to 120 μM). CDP-paratose (180−360 μM) displays competitive inhibition against CDP-3,6-dideoxy-D-*glycero*-D-*glycero*-4-hexulose and mixed type or uncompetitive inhibition with respect to NADPH. The effects of competitive dead-end inhibitors were also explored. Adenosine triphosphate ribose (73−140 μM) is a competitive inhibitor with respect to NADPH (10−140 μM) and either an uncompetitive or a mixed type inhibitor with respect to CDP-3,6-dideoxy-D-*glycero*-D-*glycero*-4-hexulose (50−410 μM). CDP (207−415 μM) is a competitive inhibitor with respect to CDP-3,6-dideoxy-D-*glycero*-D-*glycero*-4-hexulose and either an uncompetitive or a mixed type inhibitor with respect to NADPH (Table 2). It was difficult to differentiate between uncompetitive and mixed type inhibition since the lines in the Hanes−Woolf plots could be interpreted as converging on or just to the left of the *y*-axis (see Figures 4 and 5).

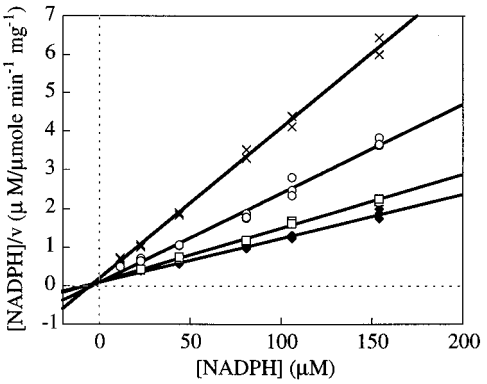

FIGURE 3: Hanes−Woolf plot of the initial velocities of CDP-paratose synthase (0.05 μg) as a function of [NADPH]. Experiments were carried out in 200 mM potassium phosphate buffer, pH 7.0, at 25 °C as described under Experimental Procedures. The NADPH concentration was varied from 10 to 150 μM at fixed levels of CDP-3,6-dideoxy-D-*glycero*-D-*glycero*-4-hexulose (**4**). The concentrations of **4** were 290 (×), 200 (○), 100 (□), and 50 μM (◆).

Table 2: Product and Dead-End Inhibition Studies

	varied substrate	
inhibitor	NADPH	**4**
$NADP^+$ [a]	competitive	uncompetitive/ mixed type
CDP-paratose[a]	uncompetitive/ mixed type	competitive
adenosine triphosphate ribose[b]	competitive	uncompetitive/ mixed type
CDP[b]	uncompetitive/ mixed type	competitive

[a] Product inhibitors. [b] Dead-end inhibitors.

Determination of K_d for NADPH. Figure 6 shows the fluorescence enhancement of NADPH upon binding to the enzyme at various NADPH concentrations. A value of $n = 2$ provides the best fit of the data to the Adair−Klotz equation (eq 4). The two dissociation constants, K_1 and K_2, derived from these data are 0.005 ± 0.002 and 12 ± 1 μM, respectively. These results reveal the existence of two cofactor binding sites per enzyme dimer where the affinity for binding of the first NADPH appears to be over 1000 times greater than for binding of the second NADPH.

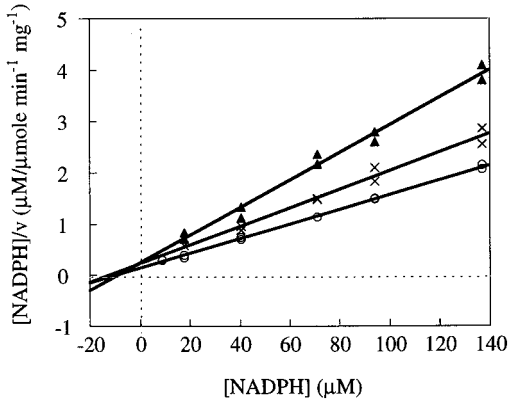

FIGURE 4: Hanes−Woolf plot of the dead-end inhibition of CDP-paratose synthase (0.05 μg) with CDP as a function of [NADPH]. Reactions were performed in 200 μM potassium phosphate buffer, pH 7.0, at 25 °C as described under Experimental Procedures. The NADPH concentration was varied between 10 and 140 μM in the presence of 170 μM CDP-3,6-dideoxy-D-*glycero*-D-*glycero*-4-hexulose. The CDP concentrations were 0 (▲), 207 (×), and 415 μM (○).

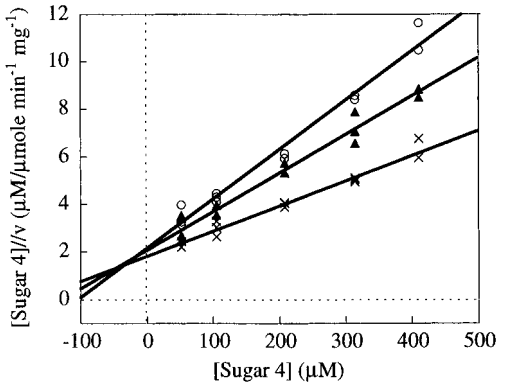

FIGURE 5: Hanes−Woolf plot of the dead-end inhibition of CDP-paratose synthase (0.05 μg) with adenosine triphosphate ribose (ATPr) as a function of [CDP-3,6-dideoxy-D-*glycero*-D-*glycero*-4-hexulose] (**4**). Reactions were performed in 200 μM potassium phosphate buffer, pH 7.0, at 25 °C as described under Experimental Procedures. The concentration of **4** was varied between 50 and 410 μM in the presence of 47 μM NADPH. The ATPr concentrations were 0 (○), 73 (▲), and 140 μM (×).

Inhibitors of CDP-paratose Synthase. The competence of various nucleotides as inhibitors for CDP-paratose synthase was tested. As shown in Table 3, CDP is the most effective inhibitor among the nucleotides examined, and it is competitive against the natural substrate (**4**) with a K_{is} of 290 ± 60 μM. In view of the K_m value of 255 μM for the natural sugar substrate (**4**), it is clear that the nucleotidyl portion is the key structural feature essential for binding. Interestingly, the substrate analogues, CDP-D-glucose (**2**) and CDP-6-deoxy-D-*glycero*-L-*threo*-4-hexulose (**3**), can inhibit this enzyme, but their inhibition is less than that of CDP alone. The latter compound **3**, which differs from the natural substrate by an additional C-3 hydroxyl group, is also a substrate, albeit an inefficient one requiring 1000 times more enzyme to achieve a comparable rate. Perhaps the extra hydroxyl at C-3 impedes the correct juxtaposition of the hexose ring in the active site, rendering hydride reduction less effective.

DISCUSSION

The NAD(P)-dependent alcohol dehydrogenases (ADHs) are an important type of oxidoreductase catalyzing the inter-

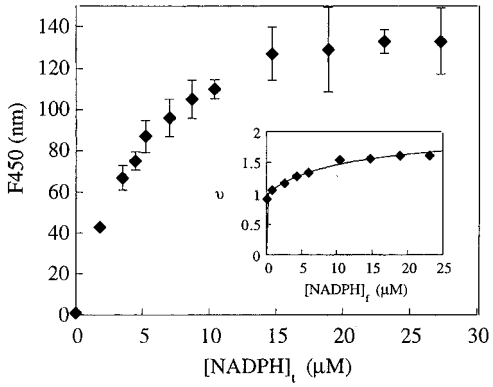

FIGURE 6: Determination of dissociation constants of NADPH based on its increased fluorescence at 450 nm upon binding with CDP-paratose synthase (2.2 μM in 200 mM potassium phosphate buffer, pH 7.0). The inset shows the plot of $\upsilon = n(I - I_i)/(I_m - I_i)$, where n represents the number of coenzyme binding sites; I_i, the initial fluorescence of the NADPH control without enzyme; and I_m, the maximum fluorescence when the NADPH concentration is infinite. The free NADPH concentration x (or $[NADPH]_f$) was estimated using $x = [NADPH]_t - n[E]_t$, in which $[NADPH]_t$ and $[E]_t$ represent total NADPH concentration and enzyme concentration, respectively. The data were fit to the Adair−Klotz equation (eq 4) using a nonlinear least squares procedure to determine the dissociation constants.

Table 3: Effect of Various Inhibitors on Activity

inhibitor	concn (mM)	% activity
CMP	1	84
CDP	1	41
CTP	1	78
ADP	1	78
CDP-glucose (**2**)	1	79
3	0.5	59

conversion between alcohols and aldehydes or ketones. This class of enzymes can be further divided into three subgroups: group I, zinc-dependent long-chain ADHs (containing approximately 350 residues per subunit); group II, short-chain zinc-independent ADHs (containing approximately 250 residues per subunit); and group III, "iron-activated" ADHs of subunit size about 385 residues (*50*). Besides the contrast in the size of their subunits and their metal dependence, a comparison of the long- and short-chain ADHs unveils a few additional differences: the long-chain ADHs usually contain the NAD(P) binding site (Rossman fold) near their C-terminus, while this motif normally resides near the N-terminus of the short-chain ADHs; reduction by the long-chain ADHs involves stereospecific transfer of the *pro-R* hydrogen from C-4′ of NAD(P)H to reduce the substrate, whereas the short-chain ADHs transfer the *pro-S* hydrogen during catalysis; and the long-chain ADHs contain a catalytic zinc atom believed to be essential for stabilization and orientation of the substrate (*50*), whereas the short-chain ADHs use a conserved Tyr and Lys to orient and activate the substrate (*51*).

CDP-paratose synthase is a dimeric protein with a small subunit size of 279 amino acids. Analysis of its sequence revealed the presence of the conserved ^{137}YXXX^{141}K motif and a NAD(P) binding fold at its N-terminus, features that are characteristic for short-chain ADHs. The stereochemical preference for transferring the *pro-S* hydrogen of NADH during catalysis further corroborates CDP-paratose synthase as a member of the short-chain ADH family. It is worth mentioning that the substrate of CDP-paratose synthase,

CDP-3,6-dideoxy-D-*glycero*-D-*glycero*-4-hexulose (**4**), can also be processed by CDP-abequose synthase (encoded by *rfbJ*) (*52*), and a very similar compound, CDP-3,6-dideoxy-D-*glycero*-L-*glycero*-4-hexulose, is the substrate for CDP-3,6-dideoxy-D-*glycero*-L-*glycero*-4-hexulose reductase (encoded by *ascF*) found in the ascarylose pathway (*18*). Examination of the *rfbJ* and *ascF* sequences show that they, too, contain the conserved Tyr and Lys residues and have the NAD(P) binding motif near their N-terminus. Similar traits were also noted for another 4-keto sugar reductase, TDP-rhamnose synthetase from the rhamnose pathway (*53*). Our recent study of the latter enzyme revealed that the hydride transfer from NADH is *pro-S* stereospecific (unpublished data). Thus, the available information suggests that all 4-keto sugar reductase may be related to the short-chain ADH family.

As a nicotinamide-dependent sugar reductase, CDP-paratose synthase displays a preference for NADP(H) over NAD(H). A recent study on the crystal structure of mouse lung carbonyl reductase, a NADPH-dependent enzyme, showed that the 2′-phosphate of NADP(H) is anchored in the active site by forming hydrogen bonds with Thr-38 through a water molecule (*54*). The significance of these interactions was demonstrated by the mutation of Thr-38 to an aspartate residue, which caused an approximately 1300-fold change in coenzyme specificity, reversing the preference for NADP(H) to NAD(H). Such a consequence has been attributed mainly to the electrostatic repulsion between the 2′-phosphate of NADP(H) and the carboxylate group of the aspartate. In a separate experiment, the importance of two positively charged residues, Lys-17 and Arg-39, in stabilizing NADPH binding with mouse lung carbonyl reductase was also established (*55*). Since Thr-38 is conserved and three corresponding positively charged residues (Arg-15, Arg-41, and Arg-43) are present in CDP-paratose synthase, the observed preference for NADP(H) is thus consistent with the prediction based on sequence alignment. Interestingly, the three aforementioned 4-keto sugar reductases all have an Asp-38 in their protein sequences; thus, these enzymes are expected to show a preference for NAD(H) in their catalysis.

While the reaction catalyzed by CDP-paratose synthase is chemically straightforward, the interpretation of the kinetic mechanism for this enzyme is complicated by its high affinity for NADPH. For example, analysis of the initial velocity data by Hanes−Woolf plots ([S]/v vs [S]) gave lines that converged on or very close to the y-axis (Figure 3). These results are consistent with either a ping-pong mechanism or a sequential mechanism with a very small K_{ia} (dissociation constant for substrate A). In the case of sequential bimolecular reactions plotted in Hanes−Woolf format, the point of intersection of the family of lines approaches the y-axis as K_{ia} approaches zero, while for a ping-pong reaction, the intersection point is located on the y-axis. When initial rate equations for ordered sequential, random sequential, and ping-pong mechanisms were fitted to the data as described in Experimental Procedures, the deduced K_{mA} and the K_{mB} for the ordered sequential equation were nearly identical with those given by the ping-pong equation since the value obtained for K_{ia} was not statistically different from zero. Therefore, the graphical analysis and the nonlinear least-squares analysis both led to the conclusion that the initial velocity data cannot be used to distinguish between a ping-pong mechanism and a sequential mechanism in this case.

A similar phenomenon was also encountered in the product inhibition studies where the Hanes−Woolf plots failed to distinguish between mixed type (lines intersect to the left of the y-axis) and uncompetitive (lines intersect on the y-axis) inhibition patterns. As shown in Table 2, our results are most consistent with either a Theorell−Chance, a ping-pong, or even a rapid equilibrium random bi-bi mechanism with dead-end EAP and EBQ complexes, where Q and P represent the products (*44*). However, the presence of both EAP and EBQ abortive complexes in a rapid equilibrium random bi-bi system seems unlikely given the large equilibrium constant ($K_{eq} = 1.6 \times 10^{12}$ M^{-1}, pH 8.0), favoring the product formation. A ping-pong mechanism also appears unlikely since it is a double-displacement reaction involving formation of covalently modified enzyme or coenzyme as an intermediate, and the absorption spectra of CDP-paratose synthase do not indicate the presence of any hydride acceptors such as cytochrome, flavin, or pyrroloquinoline quinone which have been found in some bacterial alcohol dehydrogenases (*47*). Thus, the most likely candidate is the Theorell−Chance mechanism, a special form of the ordered bi-bi mechanism where the conversion to products and release of the first product are very fast compared to release of the second product. In essence, this causes the concentration of the central complexes to be negligible and, thereby, leads to different product inhibition patterns than expected for a typical ordered bi bi mechanism.

A series of competitive dead-end inhibition experiments were also performed, but Hanes−Woolf plots of the data always gave lines that intersected so close to the y-axis that positive differentiation between uncompetitive and mixed type inhibition was difficult (Figures 4 and 5). If the reaction proceeds by an ordered mechanism, an uncompetitive inhibition pattern is predicted for the substrate that binds first in the reaction sequence. On the contrary, uncompetitive inhibition in the presence of dead-end inhibitors is anticipated for both substrates in a ping-pong mechanism. Even though the outcome of the data analysis appears to be ambiguous, the presence of a small K_{ia} would, again, explain these results.

In view of the fact that most dehydrogenases bind the nicotinamide coenzyme first, the possibility of a small K_{ia} for the binding of NADPH to CDP-paratose synthase was investigated. On the basis of the enhancement of NADPH fluorescence upon binding to the enzyme, CDP-paratose synthase was found to have two cofactor binding sites per functional dimer, and the two dissociation constants for NADPH, K_1 and K_2, are 0.005 ± 0.002 and 12 ± 1 μM, respectively. Interestingly, binding of the first NADPH exhibits a large negative cooperativity on the second binding event. Since the K_m for NADPH was determined to be 26 ± 8 μM, this value is clearly much greater than a dissociation constant (K_{ia}) of 0.005 ± 0.002 μM for NADPH. Such a small value for K_{ia} could explain all of our kinetic results and, thus, provides compelling evidence supporting a Theorell−Chance mechanism for CDP-paratose synthase (Figure 7). This mechanism is akin to those commonly encountered for the related dehydrogenase enzymes in which the nucleotide binds first, and the release of the nucleotide coenzyme is the rate-limiting step (*33*).

Table 4: Binding Sequences and NAD(P) Dissociation Constants for Some Oxido/Reductases

enzyme	source	binding sequence[a]	K_D (μM) NAD(P)$^+$	K_D (μM) NAD(P)H
CDP-paratose synthase	*S. typhi*	GAFGFLG	ND	0.005
carbonyl reductase	mouse lung	GAGKGIG	ND	1.5 (*54*)
lactate DH	killifish	VGVGAVG	ND	8.5 (*65*)
malate DH	*Thermus aquaticus*	GAAGQIG	20 (*66*)	9.5 (*66*)
polyhydroxynapthalene reductase	*Magnaporthe grisea*	GAGRGIG	38 (*67*)	31 (*67*)
glucose DH	*Bacillus subtilis*	GAASGLG	17100 (*68*)	ND
CDP-glucose 4,6-dehydratase	*Yersinia pseudotuberculosis*	GHTGFKG	0.0403 (*20*)	0.00021 (*20*)
UDP-glucose 4-epimerase	*E. coli*	GGAGYIG	very tight (*69*)	

[a] All sequences were obtained through GCG (Genetics Computer Group, Inc.).

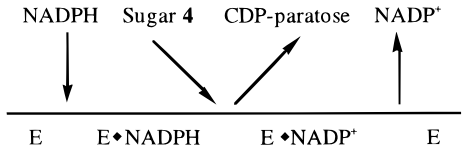

FIGURE 7: Schematic representation of the Theorell−Chance mechanism of CDP-paratose synthase.

A few other enzymes whose substrates have a small K_{ia} relative to the K_m include flavonol 3-*O*-methyltransferase from *Chrysosplenium americanum* with a K_m/K_{ia} of 23 for *S*-adenosyl-L-methionine (*56*) and human glutamic-γ-semialdehyde dehydrogenase with a K_m/K_{ia} of 25 for NAD$^+$ (*57*). Interestingly, the K_{ia} for amikacin in *E. coli* kanamycin acetyltransferase catalysis was determined to be indistinguishable from zero when amikacin was reacted with the acetyl-CoA cosubstrate (*58*). Since CDP-paratose synthase has a K_m/K_{ia} of about 5000, it is clearly a rare case with an extremely high K_m/K_{ia} ratio.

It is worth mentioning that extensive structural work has established a consensus sequence for the ADP binding motif, known as the Rossmann fold, for nicotinamide-dependent enzymes (*59*−*64*). Although almost all short-chain ADHs contain a **G**XXX**G**X**G** sequence, each of the 4-keto sugar reductases mentioned earlier has a **G**XX**G**XX**G** sequence for their NAD(P) binding sites. It has been postulated that the sequence variance within the Rossmann fold may affect the binding affinity toward NAD(P) (*20*). For example, study of CDP-D-glucose 4,6-dehydratase (E_{od}), which catalyzes the conversion of **2** to **3** using NAD$^+$ as a prosthetic group, revealed the presence of a ^{16}**G**HT**G**FK^{22}**G** binding fold, in contrast to a **G**X**G**XX**G** fold found for other dehydratases carrying a tightly bound NAD$^+$ (*20*). Interestingly, when His-17 of E_{od} was replaced by a glycine to produce a binding consensus (^{16}G**G**T**G**FK^{22}**G**) more closely resembling the **G**X**G**XX**G** sequence, an enhancement of NAD$^+$ affinity of nearly 20-fold was observed for the H17G mutant.

A comparison of the NAD(P) dissociation constants for a few representative NAD(P)-dependent dehydrogenases/reductases containing an ADP $\beta\alpha\beta$ fold of known sequence at their N-terminus showed that the binding of NADPH to CDP-paratose synthase is very tight (Table 4). Two other enzymes with higher affinity for NAD(P), UDP-glucose 4-epimerase and CDP-glucose 4,6-dehydratase, are known to use NAD(P) as a prosthetic group, not as a cosubstrate. Unfortunately, such quantitative information on enzyme−NAD(P) binding properties is only available for a limited number of proteins whose sequences are known. Thus, judgment on whether a direct correlation exists between the sequence variations of the Rossmann fold and the NAD(P) binding affinity must await a thorough comparison of more examples in this family.

In summary, the ketohexoses are important intermediates in the biosynthesis of many unusual sugars, such as deoxy sugars, branched-chain sugars, and amino sugars. The keto moiety in the precursors of these unusual sugars is catalytically pivotal since it can activate the hexose for further modification. In the formation of branched-chain sugars, branching is likely initiated by the abstraction of a proton α to the keto group to generate an enediol intermediate that is susceptible to electrophilic alkylation. Amino sugars are believed to be generated via transamination which also requires a keto functional group in the sugar precursors. Biosynthesis of the deoxy sugars commonly involves the formation of an essential keto intermediate after a dehydration step. As shown in Scheme 1, the same keto intermediate can be used in the production of several different deoxy sugars. However, the structural diversity depends on the enzymes that can perform a stereospecific reduction, therefore emphasizing the important role that each of these enzymes plays in the variation of deoxy sugars found in nature. This study on CDP-paratose synthase is the first example of a detailed characterization of this type of ketohexose reductase. Future investigations into these enzymes will establish whether CDP-paratose synthase is prototypical of this class of enzymes.

REFERENCES

1. Butterworth, R. F., and Hanessian, S. (1971) *Adv. Carbohydr. Chem. Biochem. 26*, 279−296.
2. Hanessian, S. (1966) *Adv. Carbohydr. Chem. Biochem. 21*, 143−207.
3. Williams, N. R., and Wander, J. D. (1980) in *The Carbohydrates: Chemistry and Biochemistry* (Pigman, W., and Horton, D., Eds.) Vol. 1B, pp 761−798, Academic Press, New York.
4. Ashwell, G., and Hackman, J. (1971) *Microb. Toxins 4*, 235−266.
5. Lindberg, B. (1990) *Adv. Carbohydr. Chem. Biochem. 48*, 279−318.
6. Raetz, C. R. H. (1996) in *Escherichia coli and Salmonella: Cellular and Molecular Biology* (Neidhardt, F. C., Curtiss, R., Ingraham, J. L., Lin, E. C. C., Low, K. B., Magasanik, B., Reznikoff, W. S., Riley, M., Schaechter, M., and Umbarger, H. E., Eds.) Vol. I, 2nd ed., pp 1035−1063, ASM Press, Washington, DC.
7. Lüderitz, O., Staub, A. M., and Westphal, O. (1966) *Bacteriol. Rev. 30*, 192−248.
8. Bishop, C. T., and Jennings, H. J. (1982) in *The Polysaccharides* (Aspinall, G. O., Ed.) Vol. 1, pp 291−330, Academic Press, New York.
9. Samuelsson, K., Lindberg, B., and Brubaker, R. R. (1974) *J. Bacteriol. 117*, 1010−1016.

10. Matsuhashi, S., Matsuhashi, M., and Strominger, J. L. (1966) *J. Biol. Chem. 241*, 4267−4274.
11. Gonzalez-Porque, P., and Strominger, J. L. (1972) *J. Biol. Chem. 247*, 6748−6756.
12. Rubenstein, P. A., and Strominger, J. L. (1974a) *J. Biol. Chem. 249*, 3776−3781.
13. Rubenstein, P. A., and Strominger, J. L. (1974b) *J. Biol. Chem. 249*, 3782−3788.
14. Grisebach, H. (1978) *Adv. Carbohydr. Chem. Biochem. 35*, 81−126.
15. Shibaev, V. N. (1986) *Adv. Carbohydr. Chem. Biochem. 44*, 277−339.
16. Liu, H.-w., and Thorson, J. S. (1994) *Annu. Rev. Microbiol. 48*, 223−256.
17. Heath, E. C., and Elbein, A. D. (1962) *Proc. Natl. Acad. Sci. U.S.A. 48*, 1209−1216.
18. Thorson, J. S., Lo, S. F., Ploux, O., He, X., and Liu H.-w. (1994) *J. Bacteriol. 176*, 5483−5493.
19. Yu, Y., Russell, R. N., Thorson, J. S., Liu, L.-d., and Liu, H.-w. (1992) *J. Biol. Chem. 267*, 5868−5875.
20. He, X., Thorson, J. S., and Liu, H.-w. (1996) *Biochemistry 35*, 4721−4731.
21. Weigel, T. M., Liu, L.-d., and Liu, H.-w. (1992a) *Biochemistry 31*, 2129−2139.
22. Weigel, T. M., Miller, V. P., and Liu, H.-w. (1992b) *Biochemistry 31*, 2140−2147.
23. Thorson, J. S., and Liu, H.-w. (1993) *J. Am. Chem. Soc. 115*, 7539−7540.
24. Lei, Y., Ploux, O., and Liu, H.-w. (1995) *Biochemistry 34*, 4643−4654.
25. Miller, V. P., Thorson, J. S., Ploux, O., Lo, S. F., and Liu, H.-w. (1993) *Biochemistry 32*, 11934−11942.
26. Lo, S. F., Miller, V. P., Lei, Y., Thorson, J. S., and Liu, H.-w. (1994) *J. Bacteriol. 176*, 460−468.
27. Ploux, O., Lei, Y., Vatanen, K., and Liu, H.-w. (1995) *Biochemistry 34*, 4159−4168.
28. Gassner, G. T., Johnson, D. A., Liu, H.-w., and Ballou, D. P. (1996) *Biochemistry 35*, 7752−7761.
29. Thorson, J. S., Lo, S. F., and Liu, H.-w. (1993) *J. Am. Chem. Soc. 115*, 5827−5828.
30. Matsuhashi, S., and Strominger, J. L. (1965) *Biochem. Biophys. Res. Commun. 20*, 169−175.
31. Hobbs, M., and Reeves, P. R. (1995) *Biochim. Biophys. Acta 1245*, 273−277.
32. Verma, N., and Reeves, P. (1989) *J. Bacteriol. 171*, 5694−5701.
33. Cook, P. F., and Bertagnolli, B. L. (1987) in *Pyridine Nucleotide Coenzymes: Chemical, Biochemical, and Medical Aspects, Part A* (Dolphin, D., Avramovic, O., and Poulson, R., Eds.) pp 405−448, John Wiley & Sons, New York.
34. Bradford, M. M. (1976) *Anal. Biochem. 72*, 248−254.
35. Innis, M. A., and Gelfand, D. H. (1990) in *PCR Protocols: A Guide to Methods and Applications* (Innis, M. A., Gelfand, D. H., Sninsky, J. J., and White, T. J., Eds.) pp 3−20, Academic Press, New York.
36. Sambrook, J., Fritsch, E. F., and Maniatis, T. (1989) in *Molecular Cloning: A Laboratory Manual* (Ford, N., Nolan, C., and Ferguson, M., Eds.) 2nd ed., Cold Spring Harbor Press, Cold Spring Harbor, NY.
37. Sanger, F., Nicklen, S., and Coulson, A. R. (1977) *Proc. Natl. Acad. Sci. U.S.A. 74*, 5463−5467.
38. Laemmli, U. K. (1970) *Nature 227*, 680−685.
39. Vesterberg, O. (1971) *Biochim. Biophys. Acta 243*, 345−348.
40. Andrews, P. (1964) *Biochem. J. 91*, 222−233.
41. Oppenheimer, N. J., Arnold, L. J., and Kaplan, N. O. (1971) *Proc. Natl. Acad. Sci. U.S.A.* 68, 3200−3205.
42. Gassner, G., Wang, L., Batie, C., and Ballou, D. P. (1994) *Biochemistry 33*, 12184−12193.
43. Arnold, L. J., and You, K. (1978) *Methods Enzymol. 54*, 223−232.
44. Segel, I. H. (1975) in *Enzyme Kinetics: Behavior and Analysis of Rapid Equilibrium and Steady-State Enzyme Systems*, John Wiley & Sons, New York.
45. Corbier, C., Mougin, A., Mely, Y., Adolph, H. S., Zeppezauer, M., Gerard, D., Wonacott, A., and Branlant, G. (1990) *Biochimie 72*, 545−554.
46. Clermont, S., Corbier, C., Mely, Y., Gerard, D., Wonacott, A., and Branlant, G. (1993) *Biochemistry 32*, 10178−10184.
47. MacKintosh, R. W., and Fewson, C. A. (1987) in *Enzymology and Molecular Biology of Carbonyl Metabolism III: Aldehyde Dehydrogenase, Aldo-Keto Reductase and Alcohol Dehydrogenase* (Weiner, H., and Flynn, T. G., Eds.) pp 259−273, Alan R. Liss, New York.
48. Pieper, P. A., Guo, Z., and Liu, H.-w. (1995) *J. Am. Chem. Soc. 117*, 5158−5159.
49. Gould, S. J., and Guo, J. (1992) *J. Am. Chem. Soc. 114*, 10176−10181.
50. Reid, M. F., and Fewson, C. A. (1994) *Crit. Rev. Microbiol. 20*, 13−56.
51. Jörnvall, H., Persson, B., Krook, M., Atrian, S., Gonzàlez-Duarte, R., Jeffery, J., and Ghosh, D. (1995) *Biochemistry 34*, 6003−6013.
52. Wyk, P., and Reeves, P. (1989) *J. Bacteriol. 171*, 5687−5693.
53. Jiang, X.-M., Neal, B., Santiago, F., Lee, S. J., Romana, L. K., and Reeves, P. R. (1991) *Mol. Microbiol. 5*, 695−713.
54. Nakanishi, M., Matsuura, K., Kaibe, H., Tanaka, N., Nonaka, T., Mitsui, Y., and Hara, A. (1997) *J. Biol. Chem. 272*, 2218−2222.
55. Tanaka, N., Nonaka, T., Nakanishi, M., Deyashiki, Y., Hara, A., and Mitsui, Y. (1996) *Structure 4*, 33−45.
56. de Luca, V., and Ibrahim, R. K. (1985) *Arch. Biochem. Biophys. 238*, 606−618.
57. Forte-McRobbie, C., and Pietruszko, R. (1989) *Biochem. J. 261*, 935−943.
58. Radika, K., and Northrop, D. B. (1984) *J. Biol. Chem. 259*, 12543−12546.
59. Rossmann, M. G., Liljas, A., Branden, C.-I., and Banaszak, L. J. (1975) *Enzymes (3rd Ed.) 11*, 61−102.
60. Ohlsson, I., Nordstrom, B., and Branden, C.-I. (1974) *J. Mol. Biol. 89*, 339−354.
61. Matthews, D. A., Aden, R. A., Freer, S. T., Xuong, N., and Kraut, J. (1979) *J. Biol. Chem. 254*, 4144−4151.
62. Wierenga, R. K., Drenth, J., and Schulz, G. E. (1983) *J. Mol. Biol. 167*, 725−739.
63. Wierenga, R. K., De Maeyer, M. C. H., and Hol, W. G. J. (1985) *Biochemistry 24*, 1346−1357.
64. McKie, J. H., and Douglas, K. T. (1991) *FEBS Lett. 279*, 5−8.
65. Yancey, P. H., and Siebenaller, J. F. (1987) *Biochim. Biophys. Acta 924*, 483−491.
66. Alldread, R. M., Halsall, D. M., Clarke, A. R., Sundaram, T. K., Atkinson, T., Scawen, M. D., and Nicholls, D. J. (1995) *Biochem. J. 305*, 539−548.
67. Thompson, J. E., Basarab, G. S., Andersson, A., Lindqvist, Y., and Jordan, D. B. (1997) *Biochemistry 36*, 1852−1860.
68. Hilt, W., Pfleiderer, G., and Fortnagel, P. (1991) *Biochim. Biophys. Acta 1076*, 298−304.
69. Frey, P. A. (1987) in *Pyridine Nucleotide Coenzymes: Chemical, Biochemical, and Medical Aspects, Part A* (Dolphin, D., Avramovic, O., and Poulson, R., Eds.) pp 461−597, John Wiley & Sons, New York.

BI9725529